Published online 2 December 2011 *Nucleic Acids Research, 2012, Vol. 40, No. 7* ***3245–3258***
doi:10.1093/nar/gkr1167

Crystal structure of the DNA-bound VapBC2 antitoxin/toxin pair from *Rickettsia felis*

María J. Maté[1,2], Renaud Vincentelli[1,2], Nicolas Foos[1,2], Didier Raoult[3], Christian Cambillau[1,2] and Miguel Ortiz-Lombardía[1,2,*]

[1]Aix-Marseille Université, Architecture et Fonction des Macromolécules Biologiques, Campus de Luminy, Case 932, 13288 Marseille Cedex 09, France, [2]CNRS, Architecture et Fonction des Macromolécules Biologiques, UMR6098, Campus de Luminy, Case 932, 13288 Marseille Cedex 09, France and [3]Unité des Rickettsies, CNRS UMR IRD 6236, IFR 48, Faculté de Médecine, Marseille, France

Received July 30, 2011; Revised November 11, 2011; Accepted November 13, 2011

ABSTRACT

Besides their commonly attributed role in the maintenance of low-copy number plasmids, toxin/antitoxin (TA) loci, also called 'addiction modules', have been found in chromosomes and associated to a number of biological functions such as: reduction of protein synthesis, gene regulation and retardation of cell growth under nutritional stress. The recent discovery of TA loci in obligatory intracellular species of the *Rickettsia* genus has prompted new research to establish whether they work as stress response elements or as addiction systems that might be toxic for the host cell. VapBC2 is a TA locus from *R. felis*, a pathogen responsible for flea-borne spotted fever in humans. The VapC2 toxin is a PIN-domain protein, whereas the antitoxin, VapB2, belongs to the family of swapped-hairpin β-barrel DNA-binding proteins. We have used a combination of biophysical and structural methods to characterize this new toxin/antitoxin pair. Our results show how VapB2 can block the VapC2 toxin. They provide a first structural description of the interaction between a swapped-hairpin β-barrel protein and DNA. Finally, these results suggest how the VapC2/VapB2 molar ratio can control the self-regulation of the TA locus transcription.

INTRODUCTION

Toxin–antitoxin (TA) complexes were first discovered as factors that protect low-copy number plasmids in bacteria from segregation loss (1). One protein in the pair is toxic to the cell and stable, whereas its corresponding antitoxin is unstable and requires continuous transcription to reversibly inhibit the toxin by engaging in a non-covalent complex. If the plasmid is not correctly segregated during cell division, one of the daughter cells will not carry the plasmid but will still have a number of copies of the TA complex. Eventually, the labile antitoxin will be degraded by proteases while the stable toxin will persist and kill the plasmid-free cell. In this way, the presence of TA loci prevents the proliferation of plasmid-free cells in growing bacterial cultures, and for that reason TA systems have been described as 'addiction modules'. More recently, TA loci have been associated to other biological functions such as attenuation of protein synthesis and retardation of cell growth under conditions of nutritional stress (2–4). In this regard, TA would play a role in stress physiology rather than in bacterial programmed cell death.

The most common activity of TA toxins seems to be that of an mRNA-specific endonuclease. Such activity has been already confirmed for RelE and MazF (5). VapC toxins from enteric bacteria have recently shown to specifically cleave initiator $tRNA^{fMet}$ (4). Nevertheless, two other activities have been reported: CcdB and ParE are inhibitors of DNA gyrase and the recently characterized HipA toxin is a protein kinase (6). In turn, the antitoxins consist of two domains, a C′-terminal one involved in protein–protein interactions and an N′-terminal domain responsible for DNA-binding (7,8). They belong to one of several different classes of DNA binding proteins. The binding to the toxin and to the DNA stabilizes the antitoxin, which otherwise exhibits a largely disordered structure highly susceptible to proteolysis. However, the main function of the TA binding to DNA is related to transcriptional control; TA operons are all self-regulated at the transcription level by the antitoxins, which bind to the TA operon promoters. In this respect, the toxin components can be considered as corepressors of their own transcription because TA complexes bind to DNA more strongly than antitoxins alone.

TA pairs have been classified into families based on the toxin structural features and mode of action (9). One of

*To whom correspondence should be addressed. Tel: +33 491825593; Fax: +33 491266720; Email: miguel.ortiz-lombardia@afmb.univ-mrs.fr

these, the VapBC (virulence associated protein) family, is defined by the presence of a PIN-domain protein as the toxic component (VapC). The PIN domain (PFAM: PF01850) was first annotated on the basis of sequence similarity to the N′-terminal domain of the type IV pili protein, pilT, from *Myxococcus xanthus* (PIN, PilT N′-terminus). In prokaryotes the majority of PIN-domain proteins are the toxic components of chromosomally encoded TAs. PIN-domain proteins exhibit structural homology to the T4 RNase H nuclease domain (10). Actually, the PIN-domain of the yeast Dis3 protein and the VapC toxin from enteric bacteria bear endoribonuclease activity (4,11), supporting the notion of a ribonuclease function for other PIN-domain toxins. Although sequence similarity is low within the PIN-domain, multiple-sequence alignments have shown that active site residues are highly conserved.

Other TA systems extensively studied include *Escherichia coli* MazEF and archaeal RelBE. The MazF toxin cleaves mRNA specifically at ACA sequences. The crystal structure of the MazEF complex shows a heterohexameric organization with a MazE dimer sandwiched between two MazF dimers (12). The interaction between MazE and MazF is mediated by the flexible C′-terminus of the antitoxin that wraps around the toxin homodimer. The RelE toxin is a global inhibitor of translation that is activated by nutritional stress to cleave mRNA positioned at the ribosomal A-site (13,14). RelB inhibits the action of RelE by wrapping around the toxin, thus preventing it from binding to the ribosomal A-site (15).

It is worth to note that a particular type of toxins can form TA systems with antitoxins from different protein super-families (16). Thus, the RelE/ParE toxins have been found associated with antitoxin transcriptional factors belonging to the MetJ/Arc, the PhD/YefM or the cHTH super-families. Likewise, sequence analyses have identified several PIN-domain toxins immediately adjacent to genes encoding homologues of transcriptional regulators belonging to at least four different classes, namely HTH, RHH, Phd/YefM and AbrB. These observations might indicate that TA loci have evolved through gene shuffling or partner switching (9,16).

Most of the structures of TA complexes reported so far comprise only the toxin and the C′-terminal domain of the antitoxin that wraps around it. Thus, very little structural information has been obtained concerning the N′-terminal DNA binding domain of antitoxins. The case of MazEF is an exception (12). The structure of the MazEF heterohexamer has shown that the antitoxin MazE homodimer contains an N′-terminal, intertwined β-barrel. This structure classifies MazE as a member of the large super-family of DNA binding proteins represented by the N′-terminal domain of the transcriptional factor AbrB (12, 17). Proteins from this family consist of four β-strands arranged in two anti-parallel hairpins that are interleaved in the dimer, justifying the name given to their fold: swapped-hairpin barrel.

Two crystal structures of a promoter-bound TA complex have been reported, namely those of FitAB from *Neisseria gonorrhoeae*, bound to a 36-bp DNA fragment from the fitAB promoter (7) and of *E. coli* HipAB, bound to a 21-bp operator DNA (18). The antitoxin FitA contains an N′-terminal domain with a DNA binding ribbon–helix–helix (RHH) motif, and a C′-terminal extended domain including an α-helix that interacts with the PIN-domain of the FitB toxin. Four FitA and four FitB molecules form a tetramer of heterodimers that explains why the binding to the toxin enhances the antitoxin affinity for the DNA. This structure also explains why the presence of the toxin and DNA partners stabilize the inherently flexible structure of the antitoxin. In turn, HipAB bind to DNA as a dimer of heterodimers, which also results in an enhanced DNA recognition with respect to the binding of the antitoxin alone (19).

Although well known in plasmids and in the chromosomes of free-living bacteria and archaea, the presence of TA loci was only recently confirmed in obligatory intracellular species. Thus, the complete genome sequence of *Rickettsia felis*, a flea-borne pathogen responsible for spotted fever in humans (20,21), has revealed the presence of at least 13 TA loci (22). The Rickettsia TA loci are presumed to work as addiction systems, where the elimination of TA-containing Rickettsia from host cells could lead to the release of the toxin in the cytoplasm of host, which would result in cell death (23). One of the *R. felis* TA loci includes VapC2, a protein that exhibits *in vitro* RNase activity and that can inhibit the growth of transformed *E. coli* and *S. cerevisiae* cultures (23).

We present here evidence, from multi-angle light scattering and refractometry data, for the existence of two types of *R. felis* VapBC2 complexes and reveal the structure of one of them, the octameric VapBC2 complex bound to a 27-bp dsDNA fragment from its own promoter. As in the case of FitAB, four toxins and four antitoxins form a tetramer of heterodimers that bind to the dsDNA. The toxin VapC2 contains a PIN-domain that forms homodimers homologous to those of FitB. However, the DNA-binding domain of the VapB2 antitoxin does not fold as the RHH domain of FitA. Instead, VapB2 forms homodimers that display a swapped-hairpin β-barrel fold, similar to MazE, thus illustrating the rich interplay between toxin and antitoxin super-families. Hence, this is the first structure of a TA pair composed of a toxin belonging to the VapC family and an antitoxin belonging to the AbrB/MazE superfamily. It is also the first experimental structure showing the complex of a swapped-hairpin β-barrel protein with a DNA fragment. We discuss how these data help to understand the interplay between the toxin inhibition and transcription repression functions of the antitoxin protein.

MATERIALS AND METHODS

Protein production

For expression in *E. coli*, *R. felis* vapB2 and vapC2 were cloned in operon using the Gateway (Life Technologies, Carlsbad, CA, USA) compatible destination vector pETG20A, where VapB2 was fused to thioredoxin

(TRX) at its N′-terminus to improve protein expression and solubility (24). TRX was His-tagged and followed by the tobacco virus (TEV) protease cleavage sequence, which respectively allowed affinity purification and release of the target protein.

The VapBC2 complex was expressed in BL21 Rosetta (DE3) pLysS cells (Novagen). Bacteria were grown at 37°C in auto-inducing media (25) for 4 h and transferred to 17°C when $OD_{600\,nm}$ reached ~2 (24). The selenomethionine-labelled protein was also produced using autoinducing media (25). Cultures were harvested by centrifugation at 4000*g* during 10 min and frozen at −80°C. The cell pellet was resuspended in a buffer containing 300 mM NaCl, 50 mM Tris–HCl pH 8.0, 0.25 mg/ml lysozyme, 10 mM imidazole, 20 μg/ml DNaseI, 20 mM $MgSO_4$ and a cocktail of protease inhibitors (Complete EDTA-free, Roche). Cells were disrupted by sonication and the lysate clarified by centrifugation at 20 000*g* for 30 min at 4°C.

The TA complex was loaded on a Ni^{2+}-affinity chromatography, HisTrap column (GE Healthcare) and eluted in a buffer containing 300 mM NaCl, 50 mM Tris–HCl pH 8.0 and 250 mM imidazole. After this first purification step the His-tagged thioredoxin fusion was cleaved by the addition of TEV protease. The TA complex was then recovered in the flow-through of a second Ni^{2+}-affinity chromatography.

Oligonucleotides for crystallization were annealed by slow cooling in a buffer containing 20 mM Tris–HCl (pH 8.0) and 150 mM NaCl. The sequence of the forward oligonucleotide was 5′-TTAATATATACTAAT TAATATATACTA-3′. The VapBC2 complex was mixed with the duplex DNA in a 4:1 molar ratio and purified by gel filtration in a preparative Superdex 75 HR16/60 column, using a buffer containing 25 mM Tris–HCl pH 8.0 and 150 mM NaCl.

The purity of the sample was verified by SDS–polyacrylamide gel electrophoresis on NuPAGE® Bis-Tris gels (Invitrogen).

Multiangle light scattering

The molecular weight was calculated using analytical size-exclusion chromatography (SEC) on a high-performance liquid chromatography (HPLC) system (Waters) coupled with online multiangle laser light scattering, ultra-violet light absorbance and refractive index detectors (MALLS/UV/RI) (Wyatt Technology, Santa Barbara, CA, USA). SEC was performed on a Shodex® KW-804 column with 25 mM HEPES pH 7.5, 150 mM NaCl as the eluent. The molecular weight was calculated using ASTRA V software (Wyatt Technology) with a refractive index increment (dn/dc) of 0.185 ml/g for protein samples. In the 'protein conjugate' analysis of VapBC2–DNA complexes we used extinction coefficients, at 280 nm, of 0.95 ml/(mg × cm) and 14.31 ml/(mg × cm) for VapBC2 and for the DNA, respectively. In this analysis, the refractive index increment of DNA was set to 0.166 ml/g (26).

Surface plasmon resonance

A Biacore® 1000 surface plasmon resonance system was used to study the direct binding of the VapBC2 complex to its putative cognate DNAs, as predicted from sequence analysis of the TA locus. Two different 55-mer DNA fragments, with sequences:

vapBC2_A: 5′-ATATTTAGAATAGTTGTTTGCTTTA ATAATAAAGTTAATATATACTAATT-3′
vapBC2_B: 5′-AGTTGTTTGCTTTAATAATAAAGTT AATATATACTAATTAATATATACTA-3′

were individually immobilized (332 and 268 resonance units (RU), respectively) on research grade streptavidin (SA) sensor chips. Purified VapBC2 in Tris buffer [50 mM Tris–HCl (pH 8.0), 150 mM NaCl, and 0.005% (v/v) Tween-20] was then injected at concentrations ranging from 0.25 μM to 9 μM over the immobilized DNAs at 25°C at a flow rate of 20 μl/min. Dissociation constants (K_D) were derived by non-linear curve fitting of the standard Langmuir binding isotherm using the signal at the equilibrium response level with the BIAevaluation software (version 4.1).

Complex crystallization

The VapBC2 complex bound to the 27-bp dsDNA was concentrated to 6 mg/ml. Crystals were obtained by the vapour diffusion method using a nanodrop-dispensing robot (Honeybee 961; Cartesian) in 96-well Greiner crystallization plates. The drops contained 300 nl of the complex and 100 nl of the crystallization agent, a solution of 12% PEG4000, 4% PEG400, and 100 mM MES pH 6.5. Subsequent optimizations were manually performed in 24-well plates. Crystals were very fragile, therefore cryoprotection was achieved by gradually increasing the concentration of PEG400 to 12%. The crystals were then flash-cooled in liquid nitrogen. Crystals belonged to the space group $P2_12_12_1$ with unit cell parameters $a = 80.8$ Å, $b = 92.3$ Å, whereas c was found to vary from crystal to crystal in the range of 143–164 Å. A Matthew's coefficient of 2.62, corresponding to a solvent content of 58.2%, was found to be compatible with the presence in the asymmetric unit of four TA homodimers and one molecule of double stranded DNA.

Crystal structure determination and refinement

Data were collected at the European Synchrotron Radiation Facility, ESRF (Grenoble, France). A single-wavelength anomalous diffraction (SAD) data set was collected at the Selenium peak wavelength ($\lambda = 0.9785$ Å) at beamline ID14eh4. Besides, two native data sets, from two different crystals, diffracting to 2.5 and 2.85 Å resolution were collected at beamlines ID14eh1 and ID23eh2, respectively. All data sets were reduced using XDS (27) and SCALA (28) (Table 1). The structure of the complex was solved by the SIRAS (Single Isomorphous Replacement with Anomalous Signal) method. Substructure determination, phase calculation, and density modification were carried out with autoSHARP (29) and SOLOMON (30). Phases provided by SOLOMON were

Table 1. X-ray data and refinement statistics

	SeMet data set ID14eh4	Native low resol ID23eh2	Native high resol ID14eh1
Data collection			
Space group	$P2_12_12_1$	$P2_12_12_1$	$P2_12_12_1$
Cell dimensions (Å,°)	81.5 92.9 163.4	82.0 92.8 164.1	80.8 92.3 150.5
Resolution (Å)[a]	49.0–3.5 (3.7–3.5)	49.2–2.9 (3.1–2.9)	47.3–2.5 (2.6–2.5)
No. observations			
Measured	244 369	115 005	191 495
Unique	16 251	28 411	39 577
Completeness (%)[a]	100 (98.8)	99.9 (99.9)	99.7 (99.7)
R_{meas} (%)[a]	10.9 (51.2)	9.6 (55.5)	6.6 (56.3)
Multiplicity[a]	15.0 (15.4)	4.0 (4.1)	4.9 (4.8)
$\langle\langle I\rangle/\sigma(\langle I\rangle)\rangle$[a]	23.2 (8.6)	10.9 (2.9)	17.4 (3.2)
Phasing power			
Anomalous[b]	0.935 (4.6 Å)		
Isomorphous[b,c]	0.565 (6.4 Å)		
Refinement and validation			
R_{cryst}/R_{free} (%)[d]			17.23/21.72
No. atoms: protein/DNA/water			6431/1063/360
R.m.s.d.[e]			
Bonds/angles (Å,°)			0.010/1.28
B factor (Å^2) main/side chain			2.72/6.25
Ramachandran plot[f] (# residues, %)			
Favoured regions			764, 97.7
Allowed regions			781, 99.9
Outliers			1, 0.1

[a]Values in parentheses are for the highest resolution shell.
[b]Value in parenthesis: resolution for which phasing power drops below 1.0.
[c]Isomorphous phasing power for acentric reflections using native low resolution (ID23eh2) data set.
[d]R_{free} is R_{cryst} calculated for a test set of randomly selected 5% of the data.
[e]Root mean standard deviation.
[f]Ramachandran plot statistics as reported by Molprobity (33).

introduced in BUCANEER to build an initial model of the protein components of the asymmetric unit. The rest of the model was manually built using COOT (31). The model was refined against the native data set with autoBUSTER (32) using TLS (translation/libration/screw) parameters, with one TLS group per chain. The final R_{free} is 22% and R_{cryst} is 17% (Table 1). Model validation was done with Molprobity (33). PISA (34) was used for the analysis of interfaces. Electrostatic calculations were carried out with the program APBS (35), and the electrostatic potential distribution was represented using Chimera (36), which was also used to prepare figures.

Structure deposition

Coordinates and structure factors for the DNA-bound VapBC2 complex have been deposited in the PDB under ID 3zvk.

RESULTS

The *R. felis* VapBC2 complex binds to its promoter DNA

TA complexes are known to repress the transcription of their coding genes by binding to their promoter DNA. A sequence analysis was carried out to identify possible binding sites for *R. felis* VapBC2. We aimed at finding sequence palindromes or repeats close to the TA promoter, as found in other TA operator sites (37). This analysis resulted in two possible binding sequences from the VapBC2 locus promoter that we analysed by surface plasmon resonance. One of them, vapBC2_B, displays *in vitro* good affinity with a K_D of $0.11 \pm 0.004\,\mu M$ (Figure 1a), whereas the other sequence, vapBC2_A, shows a ~40-fold higher K_D of $4.15 \pm 0.76\,\mu M$. A closer inspection of the vapBC2_B sequence revealed that the 27 most downstream bases include a nearly perfect palindrome, a hallmark of TA operator sequences (37). Therefore, we decided to pursue the rest of this study with this shorter version of the VapBC2 operator sequence.

Rickettsiae felis VapBC2 forms octamers when bound to its cognate DNA and hexamers in its absence

To gain insight into the stoichiometry of the complexes made by VapB2, VapC2 and their cognate DNA, we studied their oligomeric states by size exclusion chromatography in conjunction with multiangle light scattering (SEC/MALS). This technique allows the calculation, from MALS data, of an average molecular weight for macromolecules within each peak eluting from the SEC column. We studied first purified VapBC2 samples in the absence of DNA. Our analyses show that VapBC2 forms an 82.4 kDa complex (Figure 1b). Given the molecular masses of the VapC2 toxin (15.36 kDa) and of the VapB2 antitoxin (9.01 kDa), a number of TA ensembles are

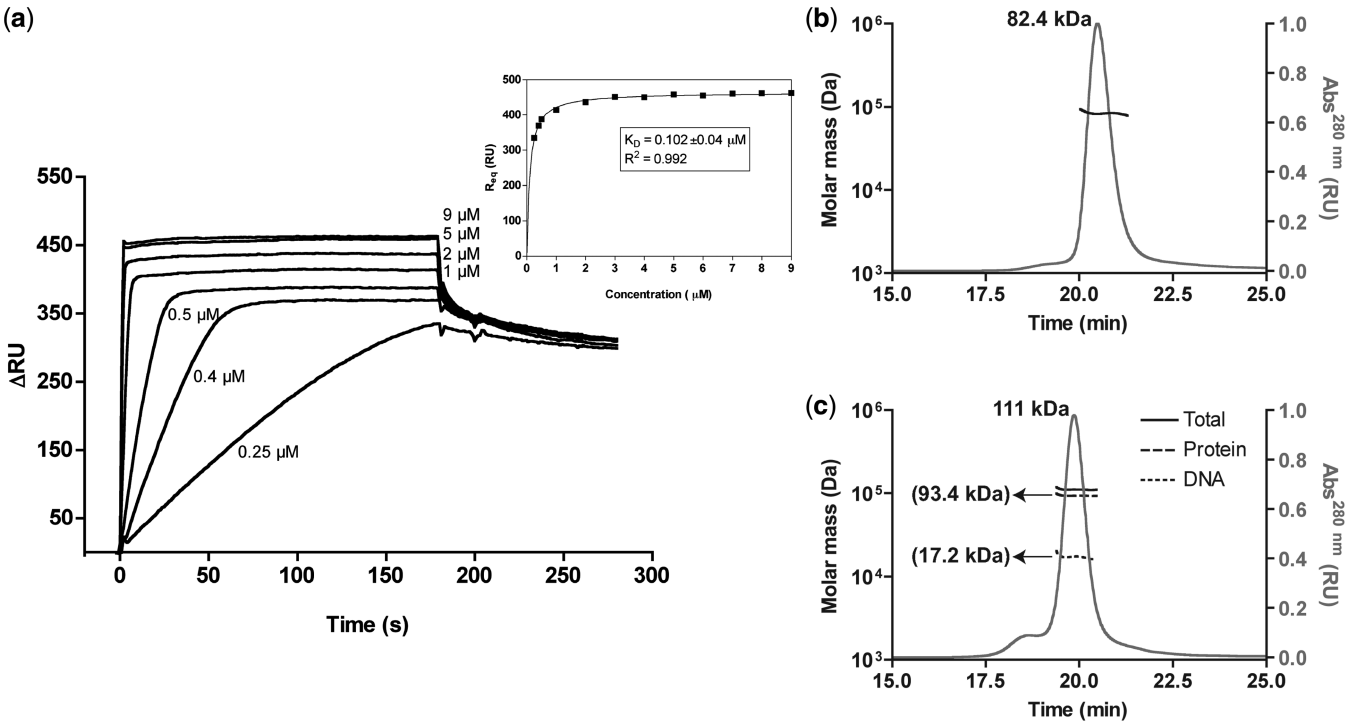

Figure 1. Analysis of the complexes formed by the VapBC2 system in the absence and presence of their cognate DNA. (**a**) SPR sensorgrams obtained by passing purified VapBC2 at the labelled concentrations (assuming an octamer) on the vapBC2_B DNA, annealed to its complement and bound to a streptavidin sensor chip. The inset shows the steady-state analysis of the binding. (**b**) About 300 μg of purified VapBC2 were subjected to size-exclusion chromatography coupled to MALS/RI/UV detectors as described in the 'Materials and Methods' section. The molar mass (black line), derived from refractive index measurements, and the absorption at 280 nm (gray line) were plotted as a function of the elution time. (**c**) Same as in (b) with 400 μg of purified VapBC2 incubated with the dsDNA used for crystallization at a 4:1 molar ratio. For clarity, the graphs of derived molar mass are only shown around the main absorption peak areas in (b) and (c). Molar mass values at the absorption peaks are indicated, with those resulting from protein-conjugate analysis in parentheses.

compatible with the measured mass within a 5% error. Among them, complexes with 3:4 (total mass 82.12 kDa) and 4:2 (79.46 kDa) stoichiometry are the likeliest ones, given the relative amounts of the proteins as observed on SDS acrylamide gels performed with the same samples. Because both molecules belong to protein families known to form homodimers, we consider the 4:2 complex as the most probable one. We also note that this stoichiometry coincides with that of the MazEF complex, which includes an antitoxin of the same family than VapB2.

Then, based on the previously known complex of the FitAB toxin with DNA, samples incubated at a 4:4:1 (VapB2:VapC2:DNA) molar ratio were also studied by SEC/MALS. In this case, the analysis of the molecular mass was carried out using the ''protein conjugate'' model, as implemented in the ASTRA software. In this method, the combined use of light scattering, ultraviolet and refractive index detectors enables the assessment of the molar mass, size, and relative polymer fractions of a copolymer such as a protein-DNA complex. With this approach, a total mass of 111 kDa breaks down into 93.41 and 17.58 kDA for the protein and DNA components, respectively (Figure 1c). These molar masses are consistent with those expected for a 4:4:1 (VapB2:VapC2:DNA) complex, 97.48 and 17.17 kDa, respectively.

Overall structure of the *R. felis* VapBC2 complex bound to its promoter DNA

We determined the structure of the VapBC2 TA complex bound to a 27-bp double stranded DNA molecule (Figure 2) by single isomorphous replacement with anomalous signal (SIRAS), using selenomethionine-substituted proteins. The final model, refined to 2.5 Å, contains four molecules of the toxin VapC2 (monomers A, B, C and D encompassing residues 1–134 for the first one and 1–133 for the other three), four molecules of the antitoxin VapB2 (monomers E, F, G and H comprising residues 2–58, 1–78, 2–77 and 1–57, respectively), 26 base pairs out of the 27 present in the double stranded DNA fragment used for crystallization, 360 molecules of water and 4 molecules of MES, the buffer used in the crystallization condition.

In a second native crystal, diffracting to 2.85 Å, all the 27-bp of the DNA fragments are visible. Whereas the crystal packing contacts are slightly different (see below), the conformation of the proteins and of the DNA are largely the same than in the structure at 2.5 Å.

The quaternary structure of the complex can be conveniently described as a tetramer of VapBC2 heterodimers bound to the DNA fragment (Figure 2a). In this regard, this complex resembles that of FitAB bound to its promoter. However, the VapBC2 complex is dramatically more compact than that of FitAB. The heterodimers

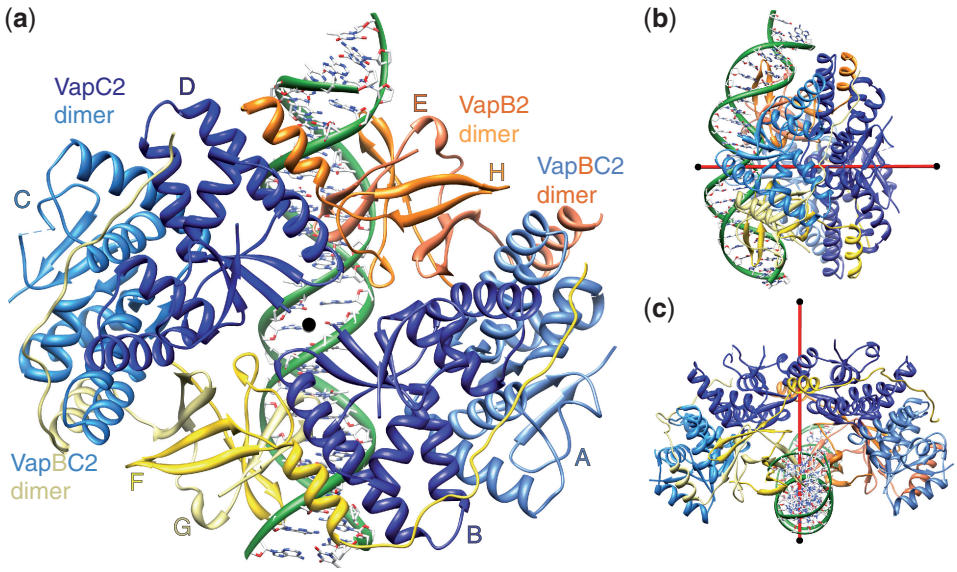

Figure 2. Three orthogonal views of the VapBC2-DNA complex. (**a**) VapB2 antitoxins are shown in different tones of blue and VapC2 toxins in yellow and orange tones. A toxin and antitoxin dimers are labelled using the colours of their components. Two toxin/antitoxin heterodimers are also marked; in one of them (bottom left) the antitoxin C′-terminus is ordered whereas in the other one (top right) it is not visible. (**b**) The DNA is significantly bent. (**c**) The VapBC2 complex interacts with the concave face of the DNA. In the three views, the pseudo-dyad axis, calculated using the two toxin homodimers as reference, is shown as a red rod with black caps.

are arranged circularly via alternative toxin–toxin and antitoxin–antitoxin dimerization interfaces. The whole VapBC2 complex has a pseudo-dyad axis, perpendicular to the DNA double helix (Figure 2). This pseudo-dyad axis intersects the DNA at the A13/T15 base pair. The interaction of the VapBC2 complex with the DNA is mediated by the two antitoxin homodimers. The interaction with DNA is described in detail below.

Structure of the VapC2 toxin

VapC2 consists of 134 amino acids forming a compact protein with an α/β/α fold. The topology of VapC2 includes 10 elements of secondary structure (Figure 3a), namely β1 (residues 2 to 5), α1 (residues 7–16), α2 (residues 19–29), β2 (residues 33–37), α3 (residues 38–50), α4 (residues 54–65), β3 (residues 69–71), α5 (residues 76–90), α6 (residues 99–109), β4 (residues 112–115), β5 (residues 128–131). A central, twisted, parallel β-sheet made of five strands (ordered 32145) is surrounded by six α-helices, with four α-helices on one side of the sheet and two on the other side. As predicted from sequence alignments VapC2 folds as a PIN-domain. This assignment was further confirmed by a search for similar structures using the DALI server (38) that gave several matches, all of them PIN-domain containing proteins. The closest structural homologues are FitB from *Neisseria gonorrhoeae* (7) (PDB: 2H1C, chain A, *Z*-score = 17.1), VapC2 (PDB ID: 3H87, chain A, $Z = 15.1$) and VapC-5 (39) (PDB ID: 3DBO, chain B, $Z = 15.0$) from *Mycobaterium tuberculosis* and two archaeal proteins (PDB: 1Y82, $Z = 15.7$; 1V96, $Z = 15.3$). PIN-domain proteins share two nearly invariant aspartic acid residues and a conserved glutamic amino-acid (40), which in VapC2 correspond to residues Asp6, Asp99 and Glu43, respectively. During the cloning a spontaneous mutation of Asp6 to glycine resulted in VapC2, perhaps inhibiting its toxic effect and allowing the overexpression of the protein.

Remarkably, VapC2 residues 116–123 (between strands β4 and β5) form a coil where other PIN-domain proteins bear a short helix, commonly described as helix α6. This helix includes a less conserved acidic residue that resides in the vicinity of the three well-conserved acidic amino acids characteristic of the domain. In VapC2, Glu120 can be regarded as the fourth acidic residue. In fact, the electron density for residues 117–124 is weak and some of them, or their side chains, could not be modelled. Indeed, this part of the model slightly differs among the four toxins. In monomers C and D this region is exposed to the solvent, and thereby less well defined than in monomers A and B.

VapC2 forms nearly symmetric homodimers that bury a solvent accessible surface area (SASA) of $1083 \pm 16\,A^2$ per monomer, representing about 14% of the total surface of the toxin (Figure 3b). The main contributions to the dimer interface arise from helices α3 and α5, which cross-interact symmetrically, and from the loop between strand β3 and helix α5. As in FitA, Phe73 (Phe78 in FitA) plays a crucial role in dimerization: its backbone carbonyl and amine atoms establish hydrogen bonds to the corresponding atoms in the other monomer. Furthermore, the backbone carbonyl of Phe73 also forms a hydrogen bond to Ser38 in the other monomer. In the same loop, Asn72 from one toxin hydrogen binds the backbone amine of Ala75 from the neighbouring toxin. Finally, Tyr46 residues make a stacking interaction with the aliphatic chains of Arg85. Besides these contacts, interactions between

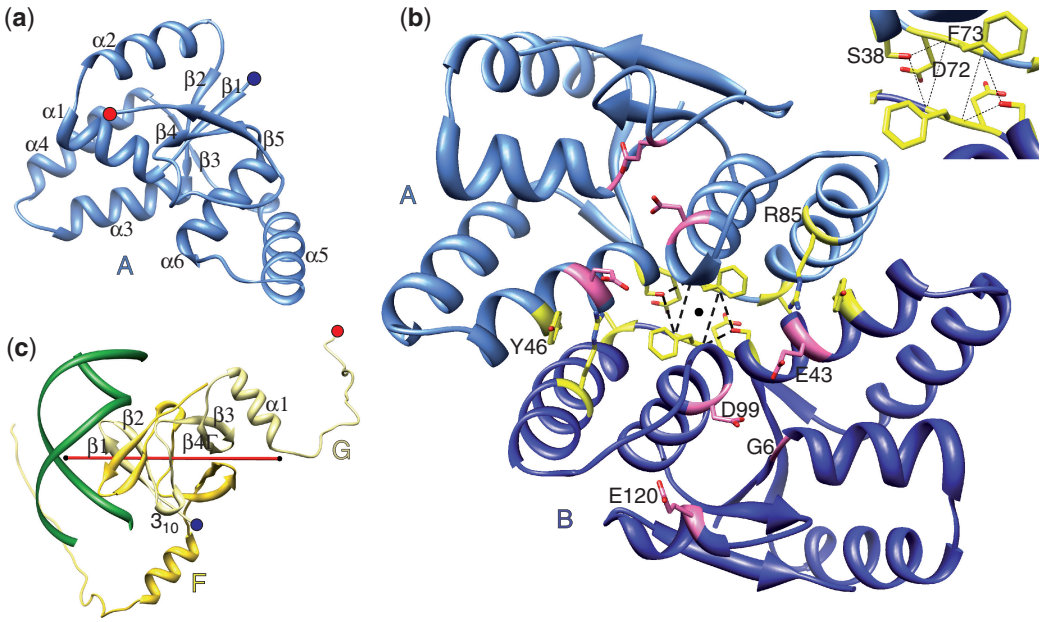

Figure 3. Structures of the VapC2 toxin and the VapB2 antitoxin in the VapBC2–DNA complex. (**a**) VapC2 toxin monomer A is shown as a ribbon diagram with labelled secondary structure elements. Blue and red circles mark the position of the N′- and C′-termini, respectively. (**b**) View of the toxin homodimer, formed by monomers A and B, along is 2-fold axis (black dot). The four acidic residues of their putative active sites are shown as sticks coloured by element, with carbons in pink. They are labelled in monomer B. Residues involved in dimerization are depicted as sticks with coloured by element, with carbons in yellow. They are labelled in monomer A. Hydrogen bonds are represented as dashed black lines. The inset gives a close-up view of the central part of the homodimer. (**c**) The antitoxin homodimer formed by monomers F and G viewed across the 2-fold axis of its β-barrel core. Secondary structure elements are labelled on monomer G. Note the asymmetry of the C′-termini with respect to the homodimer 2-fold axis. Colour codes are as in Figure 2. For simplicity, one-letter codes are used for aminoacid labels.

monomers are variable and not symmetrical. In this regard, we note that Glu43 in monomer A is involved in homodimerization contacts via a hydrogen bond to Arg85 from monomer B.

Structure of the VapB2 antitoxin

The antitoxin VapB2 consists of 78 amino acids. The secondary structure of each monomer comprises two beta-hairpins (Figure 3c): β1 (residues 6–9)/β2 (residues 12–15) and β3 (residues 28–33)/β4 (residues 36–41) connected by a loop including a short 3_{10} helix (residues 19–21) and followed by helix α1 (residues 46–55). Residues 59–78, which form an extended coil, are only visible in monomers F and G (Figure 3c). The interaction with the DNA is mediated by the β-hairpins, whereas the extended coil mediates the inhibitory interaction with VapC2 toxin homodimers (Figure 4b, see below).

Hence, the VapB2 fold differs from that of FitA (7), the cognate antitoxin of the VapC2 homologue FitB. A structure similarity search in the DALI server (38) using the N′-terminal domain of VapB2 (up to residue Pro41) yielded two main matches of medium-low statistical significance: the antitoxin MazE (12, 41) (PDB: 1MVF, chain E, *Z*-score = 4.4 and PDB: 1UB4, chain C, *Z*-score = 3.3) and the DNA binding domain of AbrB (42, 43) (PDB: 2RO4, chain B, *Z*-score = 3.1 and PDB: 1Z0R, chain A, *Z*-score = 3.0), a *B. subtilis* transcription-state regulator. This result is consistent with sequence similarity searches using BLAST against the UniProt database, which gave SpoVT/AbrB-like proteins (PFAM: PF04014) as the closest hits to VapB2. The sequence identity for the first 41 residues of VapB2 is 22% with MazE and 15% with AbrB.

It is therefore adequate to classify VapB2 in the superfamily of AbrB-like transcription factors, also called swapped-hairpin β-barrel transcription factors. Proteins of this superfamily fold as homodimeric β-barrels via two pairs of interleaved beta-hairpins (17). The only significant difference with other members of this family with known structures is that, in VapB2, the two β-hairpins are connected by a loop including a three-residues long 3_{10} helix instead of a (5–7)-residues long α-helix. Notably, the first residue in the 3_{10} helix, Lys19, and the first one after that helix, Arg22, interacts with DNA phosphates from the minor groove (see below). Structural superposition of the DNA-binding domains of VapB2, MazE (PDB: 1UB4) and AbrB (PDB: 2RO4) shows that the first β-hairpin of VapB2 is more similar to that of MazE than to that of AbrB, which is shorter. The 3_{10} helix present in VapB2 superposes to the first turn of the short helix present in MazE and AbrB. The rest of the linker is an extended coil that roughly superposes to those of MazE and AbrB (Supplementary Figure S1).

The topology of the swapped-hairpin β-barrel in the VapB2 dimers is β1, β2, β2′, β1′, β3, β4, β4′, β3′ (Figure 3c). Dimerization buries a SASA of 1589 ± 15 $Å^2$ per VapB2 monomer. This extensive dimerization interface is stabilized by a central hydrophobic core and by a network of hydrogen bonds, most of them between main-chain atoms. The interface also includes two salt bridges, Lys5-Glu27 and Asn9-Arg16.

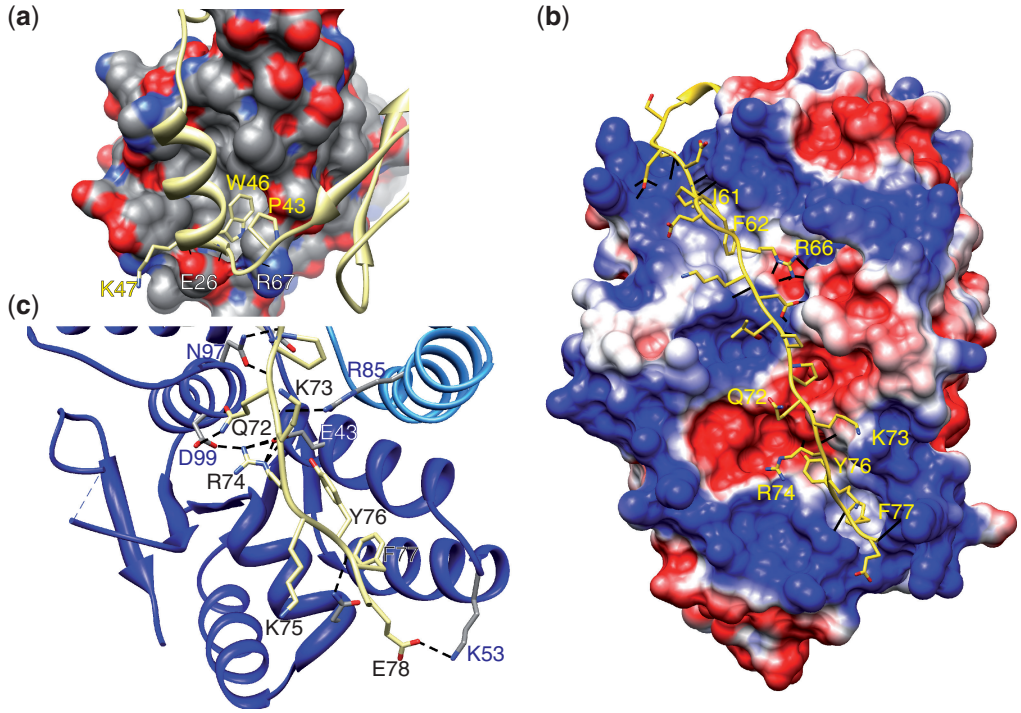

Figure 4. Antitoxin/toxin interactions. (**a**) Site 1: interaction between the antitoxin monomer G and its proximal toxin (monomer C). Residues with the strongest contributions are labelled in yellow and white for the antitoxin and the toxin, respectively. Hydrogen bonds are represented as dashed black lines. This type of interaction surface is present at all toxin/antitoxin interfaces. (**b**) Site 2: inhibitory interaction between the antitoxin monomer F and the toxin homodimer made by monomers A and B. The molecular surface of the toxin dimer is coloured by its electrostatic potential, at 150 mM ionic strength, ranging from −51 mV (red) to 51 mV (blue) at 298 K. Residues from the antitoxin are labelled in yellow. Hydrogen bonds are represented as black lines. (**c**) Site 2: a detailed view of the interaction of antitoxin monomer G with its distal toxin (monomer D, dark blue) in an orientation equivalent to that of panel b. Residues with the strongest contributions are labelled in black and blue (except for Glu43 in white) for the antitoxin and the toxin, respectively. Hydrogen bonds are represented as dashed black lines. Note the different positions and interactions of residues Arg74 and Tyr76 from the antitoxin. Colour codes are as in Figure 2. For simplicity, one-letter codes are used for aminoacid labels.

Two antitoxins suffice to block the four putative active sites of the toxins

VapB2 antitoxins interact with VapC2 toxins through two contiguous sites. In the first site (Figure 4a), the VapB2 β3/β4 hairpin, the α1 helix and the loop that connects these two elements contact helices α2 and α4 from the VapC2 toxin. All four TA heterodimers engage in this type of interaction, which buries a total area of 1739 ± 256Å^2 (941 ± 125Å^2 from VapB2 and 798 ± 132 Å^2 from VapC2). These contacts are essentially driven by van der Waals forces resulting from the interaction of the antitoxin α1 helix with a pocket defined by the toxin α2 and α4 helices, as well as by the C′-terminus of its α1 helix. Trp46 from the VapB2 antitoxin playing a dominant role, as it fills a pocket lined by residues Leu25, Glu26, Ile34, Phe64, Arg67 and Leu68 from VapC2.

A striking feature of the VapBC2 complex is that a single antitoxin is able to block the access to the two putative active sites of each toxin homodimer. This 1:2 inhibition was also found in the MazEF complex (12). The second VapC2/VapB2 interaction site (Figure 4b) involves a single antitoxin (monomers F and G) and the two toxins in a VapC2 dimer (toxin dimers AB and CD, respectively). It is noteworthy that antitoxin monomers F and G form one of the two antitoxin homodimers. Therefore, their interaction with the toxin homodimers effectively breaks the dyad symmetry of the whole VapBC2 complex. Residues 59–78 from the antitoxin mediate this type of interaction, which, contrary to the previous one, is stabilized by a dense network of polar contacts involving both main-chain and side-chain atoms. Especially noteworthy are the electrostatic contacts established by VapB2 Arg66 with residues Glu43 and Asp99 from the proximal VapC2 monomer. Contacts between the inhibitory antitoxins and the proximal toxin monomers are conserved. Conversely, contacts with the distal VapC2 monomers vary from one toxin homodimer to the other. Thus, Tyr76 from VapB2 monomer F establishes a hydrogen bond with Glu43 from the distal VapC2 monomer A. In turn, obstruction of the active site of the distal VapC2 monomer D is mainly assured by Arg74 from VapB2 monomer G, which contacts Glu43 and Asp99 from the distal toxin. Finally, in all cases VapB2 residues Ile61, Phe62, Tyr76 and Phe77 engage in van der Waals contacts that anchor the C′-terminus of the antitoxin to the surface of the toxins.

DNA conformation

DNA duplexes from adjacent asymmetric units are aligned end-to-end to form a supercoiled helix through

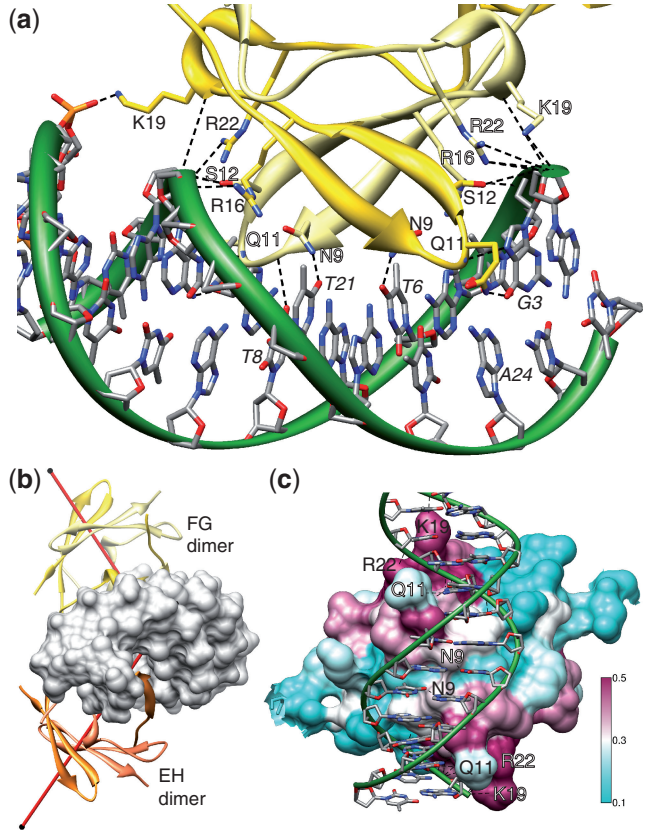

Figure 5. Antitoxin/DNA interaction. (**a**) Detail of the tight interaction of the antitoxin homodimer made by monomers F and G with the DNA. Antitoxin residues are labelled in black for monomer F and in white with a black contour for monomer G. DNA bases labels are in italics. Hydrogen bonds are represented as dashed black lines. (**b**) Overall view of the disposition of the antitoxin homodimers (only the β-barrels are shown) with respect to the DNA. The 2-fold axes of the antitoxin homodimers are shown as black-capped red rods. Colour codes are as in Figure 2. For simplicity, one-letter codes are used for aminoacid labels. (**c**) Sequence conservation in the swapped-hairpin β-barrel domain at the DNA interface. The sequence of VapB2 was aligned with the Pfam representative set of sequences for the PF04014 family using Muscle (58). Conservation was mapped onto the molecular surface of the VapB2 homodimer FG (residues 1–45) using the identity histogram model implemented in Chimera (36). Protein residue labels are as in panel a. A colour key bar shows the colour correspondence for lower (cyan) to higher (maroon) conservation.

the crystal lattice. The supercoil results from an overall bend of 36.8°, as calculated by CURVES (44) (Figure 2b). Bending is maximal in the central part of the DNA and as a result, the molecule offers a concave surface to the interaction with the VapBC2 complex (Figures 2b and 5b).

The most remarkable feature of structure of this DNA is that the minor groove in the AT-rich central region (bases 13–16, forward chain) is severely compressed, shrinking to less than half the width of canonical B-DNA: 2.6 Å for base-pairs A13/T15 and A14/T14, compared to the standard 6 Å. In contrast, the minor groove width increases to 8.5–8.7 Å in the region directly interacting with VapB2 (bases 3–11 and 18–26, forward chain). The minor groove is again compressed at the DNA ends, presumably due to crystal packing forces. The oscillations in the minor groove width correlate with changes in the width of the major groove. However, all along the DNA molecule, the major groove is wider than in a canonical B-DNA (11.5 Å). Thus, in the centre of the fragment the major groove width is ~12.4 Å, whereas in the VapB2-interacting area it increases to ~15.5 Å (Supplementary Figure S2).

Interaction of the antitoxins VapB2 with DNA

The sequence of the vapBC2 promoter used in this study includes an imperfect palindrome spanning from base T2 to base T27 (forward sequence), with half-sequence TA(A/G)TATATA(C/T)TAA. Within this palindrome, two regions are directly recognized by the antitoxin homodimers: base-pairs A3/T25 to T12/A16 by the EH VapB2 dimer and base-pairs A17/T11 to G26/A2 by the FG VapB2 dimer (Figure 5a). Since each of these regions is recognized by an antitoxin homodimer, it is not surprising to note that they are also internally nearly palindromic (Figure 2), being A(A/G)TAT their half-sequence.

Globally, the VapB2 homodimers interact with the concave face of the curved DNA: when looking at the complex along overall longitudinal axis of the DNA, the dyad axes of the two antitoxin homodimers make an angle of ~110° (Figure 5b). In the VapB2 homodimers the first β-hairpins from each antitoxin (strands β1 and β2) form together a saddle-shaped surface that deeply penetrates the DNA major grove (Figure 5a), providing a strong hydrophobic base to the interaction. A total 1151 ± 7 $Å^2$ area is buried by the interaction of each antitoxin homodimer with a half site, resulting in a solvation energy gain of $-14\,kcal\,mol^{-1}$, as estimated by PISA (34). Two residues, Asn9 and Gln11, make specific hydrogen bonds with the DNA bases. The Asn9 residues, which are at the C′-terminus of the β1 strand, contact the central base-pairs while the Gln11 residues, in the β1-β2 loop, contact the penultimate base-pairs of the pseudo-palindromic interacting regions. The Asn9 residues specifically recognize the O4 positions of the thymidines belonging to the central base-pairs. The position of Asn9 is stabilized by the Arg16 residue from the same antitoxin, which in turn contacts the DNA backbone, thus contributing to the opening of the major groove. The role of Gln11 is particularly interesting since it adjusts to the adenine/guanine variability within the palindrome recognized by each antitoxin dimer. Indeed, the side-chain amide group of a glutamine residue interacts equally well with the N6 of an adenine or with the O6 of a guanine. Besides these contacts, the main-chain amine from each Gln11 recognizes the N7 position, common to adenines and guanines. Finally, residues Lys19, from the 3_{10} helix between strands β2 and β3, and Arg22, in the loop that follows that helix, further contribute to stabilize the antitoxin–DNA interaction through electrostatic contacts with the DNA phosphate backbone. A full map of the VapB2/DNA contacts is available in Suppl. Figure 3.

Sequence conservation in the swapped-hairpin β-barrel DNA binding domain is consistent with the different roles of the β2–β3 and the β1–β2 loops. Thus, the DNA backbone binding residues in the β2–β3 loop are the most conserved at the interface with DNA. Conversely, residues in the β1–β2 loop region, which make direct base-specific residues and so drive the recognition of a particular sequence, are less conserved (Figure 5c).

DISCUSSION

A $(VapC2)_4(VapB2)_2$ heterohexamer likely constitutes the toxin-inhibited complex whereas a $(VapC2)_4(VapB2)_4$ heterooctamer binds to the locus operator DNA

PIN domains resemble structurally to the T4 RNaseH (10). In keeping with this observation, the PIN domain of the eukaryotic exosomal protein Rrp44 displays endoribonucleolytic activity (11) and VapC toxins from enteric bacteria specifically cleave the initiator $tRNA^{fMet}$ (4). The three conserved acidic residues of the PIN domain are clustered at the surface of the protein and superpose well to part of the active site of the T4 RNaseH, namely RNaseH residues Asp19, Asp71 and Asp132. In VapC2 these residues correspond to amino acids Asp6, Asp99 and Glu43, respectively (Figure 3b). In the structure described in this work Asp6 is mutated to glycine. An Asp→Ala substitution in the equivalent residue (Asp7) of an enteric VapC toxin resulted in an inactive enzyme *in vivo* (4). We infer that the VapC2 protein in our construct is also inactive.

A fourth acidic residue is present in PIN domains. Its position at the sequence level can vary from a protein to another, as it lies in a region structurally more variable than the former three residues. Glu120, which sits in a flexible loop that in other PIN domains folds as a short helix, is the likely candidate for this fourth acidic residue in VapC2. Actually, the side chain of Glu120 could only be fully modelled in monomer A, where it is hydrogen bound to residues Thr115 and Asn8 from the same monomer. The larger active site of T4 RNaseH coordinates two divalent metal cations whereas, in principle, the active site of PIN domains could bind one. Nevertheless, in line with other known structures of PIN domain proteins, that of VapC2 in the VapBC2–DNA complex does not include any metal cation. The Asp6Gly point mutation present in our VapC2 construct is a likely explanation for this absence. Notwithstanding, it is also possible that the enzymatic mechanism of VapC2 does not imply metal cofactors, that they may have been displaced by the interaction with the antitoxin or that the metals are only transiently bound to the enzyme during the reaction.

Globally, the putative active site of VapC2 resides on a surface pocket near the dimerization interface of the toxin homodimer; therefore, both active sites are close to each other. In fact, they are connected by a groove that spans the full length of the toxin homodimer. In the structure of VapBC2 this groove is filled by one antitoxin C′-terminus. However, it is clear that a putative RNA substrate would also fit. Consistent with this hypothesis, the groove presents an overall positive charge, except for the active site pockets. Since the rest of the dimer bears a negative electrostatic potential, the groove could aptly attract a negatively charged substrate such as an RNA fragment. Based on the fact that the VapB2 anti-toxin blocks the access to the putative active and substrate-binding sites of VapC2, we propose that this mode of interaction corresponds to the toxin-inhibited complex.

In the other structurally characterized TA complexes involving PIN-domain toxins, namely *N. gonorrhoeae* FitAB and *M. tuberculosis* VapBC-5, each toxin active site is blocked in a topologically similar way, that is, by occlusion of the active and substrate-binding sites (Supplementary Figure S4), further supporting our hypothesis that the VapB2/VapC2 interaction that we see corresponds to the toxin-inhibited complex. In the FitAB structure, each FitB toxin monomer is blocked by one FitA antitoxin monomer (7). Yet, in the case of *R. felis* VapBC2, a single VapB2 antitoxin monomer suffices to occlude the two active sites of a VapC2 toxin homodimer. This situation is reminiscent of the MazEF complex, where a single monomer of MazE, a swapped-hairpin β-barrel antitoxin similar to VapB2, interacts with both monomers of a MazF toxin homodimer (12). We suggest that this interaction scheme, observed in complexes with two different types of toxins, might be a characteristic trait of swapped-hairpin β-barrel DNA-binding antitoxins. The molecular characterization of other TA pairs involving swapped-hairpin β-barrel antitoxins will be needed to confirm this hypothesis.

Notwithstanding, the significance of this finding can be better understood in view of our SEC/MALS results, which shows that VapbC2:VapB2 stoichiometry changes from 4:2 to 4:4 upon binding to DNA. In the absence of their cognate DNA, MazE and MazF form a heterohexamer comprising two MazF toxin homodimers and a MazE antitoxin homodimer (12). A 4:2 stoichiometry had also been inferred for the ccdAB toxin–antitoxin system (45). However, in the presence of their target DNA ccdAB would form oligomeric species with a 1:1 molar ratio (45,46). Hence, it seems conceivable that, at least for toxin–antitoxin systems involving swapped-hairpin β-barrel DNA-binding antitoxins, the complexes required for toxin inhibition and for transcription self-repression differ. Thus, our data transposes to *R. felis* VapBC2 and, at the same time rationalizes, the model first proposed for the CcdAB system (46) (Figure 5). In these operons the antitoxin genes are coded upstream the toxin ones, therefore antitoxins will be likely produced at higher levels than their cognate toxins. However, the antitoxins' high susceptibility to proteases will compensate and eventually revert this advantage. While the levels of toxin and antitoxin are high enough and close to a 1:1 molar ratio, they will form complexes able to repress their own transcription. At some point, the levels of antitoxin may decrease so that such complexes are no longer favoured but still there are enough antitoxin molecules to inhibit the more stable toxins. Then, if the coding DNA is still present, transcription can resume before antitoxin levels decay so much that toxins can poison the host cell. Hence, the fact that the toxin-inhibitory and the

transcriptional repressor complexes bear a different stoichiometry adds a further level of control to the TA system.

DNA sequence and toxin/antitoxin interfaces drive the recognition of the locus operator by the VapBC2 complex

The recognition of specific DNA sequences by proteins depends on two types of readout mechanisms that complement each other to assure specificity and affinity. The first recognized mechanism is the so-called 'direct' or 'base' readout that involves the formation of hydrogen bonds with specific bases, primarily in the major groove. A second mechanism was subsequently identified and dubbed 'indirect' or 'shape' readout (47,48). Shape readout depends on the propensity of a given DNA sequence to assume a conformation that facilitates its binding to a particular protein. The nucleotides involved in shape readout do not need to be in contact with the protein. Indeed, they are often in linker sequences connecting two half-sites that bind to different protein subunits. Such is the case of the A-tract in the core region of the sequence recognized by the cancer-associated human papillomavirus E2 protein (49). We find a similar situation in the AT-rich promoter region recognized by the VapBC2 complex, which includes a central linker region that separates the two half-sites contacted by the antitoxin homodimers. In AT-rich sequences, ApT and ApA (TpT) base pair steps usually display negative roll angles that lead to a compression of the minor groove (50). We do observe negative roll angle values between bases 12 and 16 in the central region (Supplementary Figure S2), which result in a severely compressed minor groove in this region. Conversely, TpA steps act as 'hinge steps' that tend to compress the major groove and provide a higher deformability that can affect the entropy of complex formation (51). In the DNA bound to VapBC2, two TpA steps, T11pA12 and T15pA16, separate the central, minor-groove-compressed region from the binding half-sites, which are themselves rich in TpA steps and therefore more deformable. Compression of the DNA minor groove is widely found in protein-DNA recognition, where it can serve other purposes than modifying the DNA shape. Thus, narrow minor grooves locally enhance the negative electrostatic potential of DNA and, in that way, they attract positively charged amino acids, preferably arginines, into the minor groove (52,53). In the VapBC2–DNA complex, the amino groups of two lysines, residues Lys19 from the VapB2 molecules F and H, do contact the phosphate backbone from the central minor groove of the target DNA.

We conclude that the central compression of the DNA minor groove, combined with deformable binding half-sites, enables the antitoxin to insert into adjacent major grooves in the concave face of the bent DNA. This is reminiscent of the binding mechanism by which the Fis protein selects DNA targets based on the intrinsic width of the minor groove, using the separation between helix–turn–helix (HTH) motifs as a ruler (54). However, the structure that we have solved shows that the VapBC2 complex actively participates in this adaptation process: the VapBC2 complex is not perfectly 2-fold symmetrical, showing a 175° rotation, instead of 180°, between the two toxin homodimers. This slight asymmetry reflects the need of this complex to adapt to the relative positions of the half-sites and strongly supports the notion that a combination of DNA and protein properties is needed to allow their mutual recognition and eventual interaction. To better understand the source of this asymmetry, we must consider the fact that a VapBC2 hexameric complex exists in solution in the absence of DNA. At least for the CcdAB, Phd/doc and ParDE systems, a high toxin:antitoxin ratio would lift DNA binding or transcriptional repression (46,55–57). Although we have not determined this behaviour in the case of VapBC2, it is plausible that VapBC2 hexamers cannot bind DNA, or

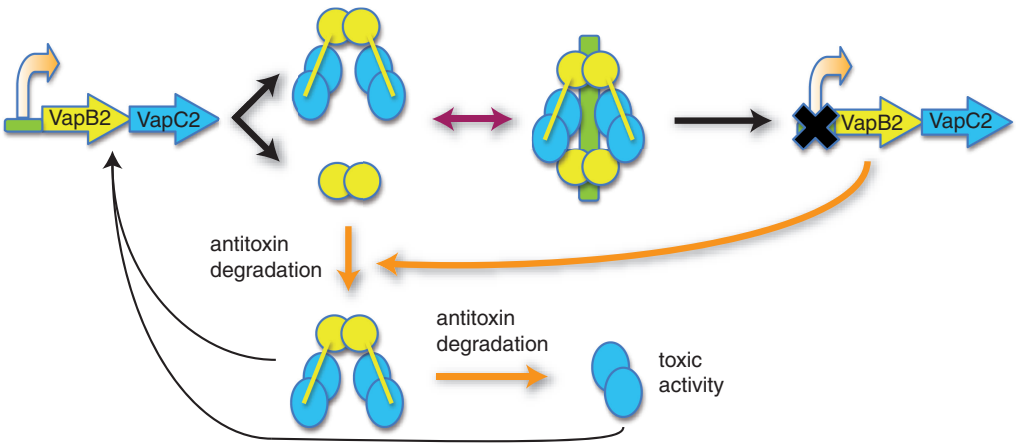

Figure 6. Proposed model for the regulation by stoichiometry of the transcription control and toxic activities in the VapBC2 system. Transcription of the VapBC2 locus results in the production of both heterohexameric $(VapB2)_2(VapC2)_4$ and homodimeric $(VapB2)_2$ complexes. These complexes would cooperatively bind to the locus promoter DNA, down-regulating its transcription in a negative feedback. The higher susceptibility to proteolysis of the antitoxin will result in an excess of $(VapB2)_2(VapC2)_4$ hexamers and hence in derepression of the promoter DNA and production of fresh toxin and antitoxin proteins. However, if the DNA coding the VapBC2 has disappeared, or is otherwise repressed, the depleted antitoxin will not be replaced. Eventually, further degradation of the antitoxin will allow the toxin dimers to freely degrade their substrates. The C′-termini of the antitoxins in the $(VapB2)_2$ homodimers are not depicted to denote their presumable high disorder or propensity to proteolysis.

bind to it with lower affinity than VapB2 antitoxin homodimers. One could then hypothesize that while the toxin:antitoxin ratio is kept low, VapBC2 heterohexamers and VapB2 homodimers would coexist. In this scenario, VapB2 homodimers would bind to the recognition half-sites of their cognate DNA, from where they could recruit VapBC2 hexamers to form a fully active repression complex. The antitoxin hinge region (residues Pro41 to Asn44) is likely to play a major role in the adaptation of the VapBC2 full complex to its cognate DNA. Finally, when the levels of antitoxin dwindle, VapBC2 hexamers will prevail, bind with lower affinity, or not at all to the DNA and repression will be lifted, so that the toxin:antitoxin ratio can be re-equilibrated (Figure 6).

CONCLUSION

The study of the VapBC2 system has provided new insights into the mechanisms that underlie toxin inhibition by antitoxins of the swapped-hairpin β-barrel family. Furthermore, our combination of biophysical and structural methods has shed light onto how the different complexes formed by VapB2 and VapC2, but possibly also by other toxin/antitoxin pairs, integrate the control of the toxin activity with their participation in the regulation of their own transcription.

This work represents as well the first experimental structure of a protein from the swapped-hairpin β-barrel family bound to DNA. The structure essentially confirms previous models based on the unbound structures of MazE (41) and AbrB (42), while providing a first detailed view of the contacts involved in DNA binding. Indeed, the structure underlines the importance of a large interaction surface that results in a marked widening of the DNA major groove, which combined with the relative positioning of the VapB2 antitoxin homodimers in the context of the complex, possibly enhances the bending of the DNA. Thus, the mutual adjustments between an intrinsically bendable DNA and the VapB2/VapC2 interfaces, both within the VapBC2 heterohexamer and between this complex and the DNA-bound VapB2 homodimer, may explain the increased affinity of the ternary toxin–antitoxin–DNA complex.

ACCESSION NUMBER

3zvk.

SUPPLEMENTARY DATA

Supplementary Data are available at NAR Online: Supplementary Figures S1–S4 and Supplementary Reference [59].

ACKNOWLEDGEMENTS

The authors thank Gregory Gimenez for suggesting possible sequences for the VapBC2 locus promoter, Stéphanie Blangy and Catarina Rodrigues for their assistance with SEC/MALS experiments, Mariella Tegoni for help with the SPR assays and Gilles Audoly for helpful discussions. They also thank the staff of the ID14eh1, ID14eh4 and ID23eh2 beamlines at the European Synchrotron Radiation Facility (ESRF; Grenoble, France) for their help and support.

FUNDING

The Ville de Marseille provided a financial installation aid (to M.O.-L.). M.J.M. was supported by the Fondation Infectiopôle Sud. Funding for open access charge: Internal Resources.

Conflict of interest statement. None declared.

REFERENCES

1. Gerdes,K., Rasmussen,P.B. and Molin,S. (1986) Unique type of plasmid maintenance function: postsegregational killing of plasmid-free cells. *Proc. Natl Acad. Sci. USA*, **83**, 3116–3120.
2. Pedersen,K., Christensen,S.K. and Gerdes,K. (2002) Rapid induction and reversal of a bacteriostatic condition by controlled expression of toxins and antitoxins. *Mol. Microbiol.*, **45**, 501–510.
3. Gerdes,K. (2000) Toxin-antitoxin modules may regulate synthesis of macromolecules during nutritional stress. *J. Bacteriol.*, **182**, 561–572.
4. Winther,K.S. and Gerdes,K. (2011) Enteric virulence associated protein VapC inhibits translation by cleavage of initiator tRNA. *Proc. Natl Acad. Sci. USA*, **108**, 7403–7407.
5. Yamaguchi,Y. and Inouye,M. (2009) mRNA interferases, sequence-specific endoribonucleases from the toxin-antitoxin systems. *Prog. Mol. Biol. Transl. Sci.*, **85**, 467–500.
6. Correia,F.F., D'Onofrio,A., Rejtar,T., Li,L., Karger,B.L., Makarova,K., Koonin,E.V. and Lewis,K. (2006) Kinase activity of overexpressed HipA is required for growth arrest and multidrug tolerance in *Escherichia coli*. *J. Bacteriol.*, **188**, 8360–8367.
7. Mattison,K., Wilbur,J.S., So,M. and Brennan,R.G. (2006) Structure of FitAB from *Neisseria gonorrhoeae* bound to DNA reveals a tetramer of toxin-antitoxin heterodimers containing pin domains and ribbon-helix-helix motifs. *J. Biol. Chem.*, **281**, 37942–37951.
8. Wilbur,J.S., Chivers,P.T., Mattison,K., Potter,L., Brennan,R.G. and So,M. (2005) *Neisseria gonorrhoeae* FitA interacts with FitB to bind DNA through its ribbon-helix-helix motif. *Biochemistry*, **44**, 12515–12524.
9. Gerdes,K., Christensen,S.K. and Løbner-Olesen,A. (2005) Prokaryotic toxin-antitoxin stress response loci. *Nat. Rev. Microbiol.*, **3**, 371–382.
10. Arcus,V.L., Bäckbro,K., Roos,A., Daniel,E.L. and Baker,E.N. (2004) Distant structural homology leads to the functional characterization of an archaeal PIN domain as an exonuclease. *J. Biol. Chem.*, **279**, 16471–16478.
11. Lebreton,A., Tomecki,R., Dziembowski,A. and Séraphin,B. (2008) Endonucleolytic RNA cleavage by a eukaryotic exosome. *Nature*, **456**, 993–996.
12. Kamada,K., Hanaoka,F. and Burley,S.K. (2003) Crystal structure of the MazE/MazF complex: molecular bases of antidote-toxin recognition. *Mol. Cell*, **11**, 875–884.
13. Christensen,S.K. and Gerdes,K. (2003) RelE toxins from bacteria and Archaea cleave mRNAs on translating ribosomes, which are rescued by tmRNA. *Mol. Microbiol.*, **48**, 1389–1400.
14. Pedersen,K., Zavialov,A.V., Pavlov,M.Y., Elf,J., Gerdes,K. and Ehrenberg,M. (2003) The bacterial toxin RelE displays codon-specific cleavage of mRNAs in the ribosomal A site. *Cell*, **112**, 131–140.
15. Takagi,H., Kakuta,Y., Okada,T., Yao,M., Tanaka,I. and Kimura,M. (2005) Crystal structure of archaeal toxin-antitoxin RelE-RelB complex with implications for toxin activity and antitoxin effects. *Nat. Struct. Mol. Biol.*, **12**, 327–331.

16. Anantharaman,V. and Aravind,L. (2003) New connections in the prokaryotic toxin-antitoxin network: relationship with the eukaryotic nonsense-mediated RNA decay system. *Genome Biol.*, **4**, R81.
17. Coles,M., Djuranovic,S., Söding,J., Frickey,T., Koretke,K., Truffault,V., Martin,J. and Lupas,A.N. (2005) AbrB-like transcription factors assume a swapped hairpin fold that is evolutionarily related to double-psi beta barrels. *Structure*, **13**, 919–928.
18. Schumacher,M.A., Piro,K.M., Xu,W., Hansen,S., Lewis,K. and Brennan,R.G. (2009) Molecular mechanisms of HipA-mediated multidrug tolerance and its neutralization by HipB. *Science*, **323**, 396–401.
19. Black,D.S., Kelly,A.J., Mardis,M.J. and Moyed,H.S. (1991) Structure and organization of hip, an operon that affects lethality due to inhibition of peptidoglycan or DNA synthesis. *J. Bacteriol.*, **173**, 5732–5739.
20. La Scola,B., Meconi,S., Fenollar,F., Rolain,J.-M., Roux,V. and Raoult,D. (2002) Emended description of *Rickettsia felis* (Bouyer et al. 2001), a temperature-dependent cultured bacterium. *Int. J. Syst. Evol. Microbiol.*, **52**, 2035–2041.
21. Raoult,D., La Scola,B., Enea,M., Fournier,P.E., Roux,V., Fenollar,F., Galvao,M.A. and de Lamballerie,X. (2001) A flea-associated Rickettsia pathogenic for humans. *Emerg. Infect. Dis.*, **7**, 73–81.
22. Ogata,H., Renesto,P., Audic,S., Robert,C., Blanc,G., Fournier,P.-E., Parinello,H., Claverie,J.-M. and Raoult,D. (2005) The genome sequence of *Rickettsia felis* identifies the first putative conjugative plasmid in an obligate intracellular parasite. *PLoS Biol.*, **3**, e248.
23. Audoly,G., Vincentelli,R., Edouard,S., Georgiades,K., Mediannikov,O., Gimenez,G., Socolovschi,C., Mège,J.-L., Cambillau,C. and Raoult,D. (2011) Toxic effect of rickettsial toxin VapC on its eukaryotic host. *PLoS ONE*, **6**, e26528.
24. Vincentelli,R., Cimino,A., Geerlof,A., Kubo,A., Satou,Y. and Cambillau,C. (2011) High-throughput protein expression screening and purification in *Escherichia coli*. *Methods*, **55**, 65–72.
25. Studier,F.W. (2005) Protein production by auto-induction in high density shaking cultures. *Protein Expr. Purif.*, **41**, 207–234.
26. Krasna,A.I., Dawson,J.R. and Harpst,J.A. (1970) Characterization of acid-denatured DNA by low-angle light scattering. *Biopolymers*, **9**, 1017–1028.
27. Kabsch,W. (2010) XDS. *Acta Crystallogr. D Biol. Crystallogr.*, **66**, 125–132.
28. Evans,P. (2006) Scaling and assessment of data quality. *Acta Crystallogr. D Biol. Crystallogr.*, **62**, 72–82.
29. Vonrhein,C., Blanc,E., Roversi,P. and Bricogne,G. (2007) Automated structure solution with autoSHARP. *Methods Mol. Biol.*, **364**, 215–230.
30. Abrahams,J.P. and Leslie,A.G. (1996) Methods used in the structure determination of bovine mitochondrial F1 ATPase. *Acta Crystallogr. D Biol. Crystallogr.*, **52**, 30–42.
31. Emsley,P., Lohkamp,B., Scott,W.G. and Cowtan,K. (2010) Features and development of Coot. *Acta Crystallogr. D Biol. Crystallogr.*, **66**, 486–501.
32. Blanc,E., Roversi,P., Vonrhein,C., Flensburg,C., Lea,S.M. and Bricogne,G. (2004) Refinement of severely incomplete structures with maximum likelihood in BUSTER-TNT. *Acta Crystallogr. D Biol. Crystallogr.*, **60**, 2210–2221.
33. Davis,I.W., Leaver-Fay,A., Chen,V.B., Block,J.N., Kapral,G.J., Wang,X., Murray,L.W., Arendall,W.B. III, Snoeyink,J., Richardson,J.S. *et al.* (2007) MolProbity: all-atom contacts and structure validation for proteins and nucleic acids. *Nucleic Acids Res.*, **35**, W375–W383.
34. Krissinel,E. and Henrick,K. (2007) Inference of macromolecular assemblies from crystalline state. *J. Mol. Biol.*, **372**, 774–797.
35. Baker,N.A., Sept,D., Joseph,S., Holst,M.J. and McCammon,J.A. (2001) Electrostatics of nanosystems: application to microtubules and the ribosome. *Proc. Natl Acad. Sci. USA*, **98**, 10037–10041.
36. Pettersen,E.F., Goddard,T.D., Huang,C.C., Couch,G.S., Greenblatt,D.M., Meng,E.C. and Ferrin,T.E. (2004) UCSF Chimera—a visualization system for exploratory research and analysis. *J. Comput. Chem.*, **25**, 1605–1612.
37. Bailey,S.E.S. and Hayes,F. (2009) Influence of operator site geometry on transcriptional control by the YefM-YoeB toxin-antitoxin complex. *J. Bacteriol.*, **191**, 762–772.
38. Holm,L. and Rosenström,P. (2010) Dali server: conservation mapping in 3D. *Nucleic Acids Res.*, **38**, W545–W549.
39. Miallau,L., Faller,M., Chiang,J., Arbing,M., Guo,F., Cascio,D. and Eisenberg,D. (2009) Structure and proposed activity of a member of the VapBC family of toxin-antitoxin systems. VapBC-5 from *Mycobacterium tuberculosis*. *J. Biol. Chem.*, **284**, 276–283.
40. Makarova,K.S., Aravind,L., Galperin,M.Y., Grishin,N.V., Tatusov,R.L., Wolf,Y.I. and Koonin,E.V. (1999) Comparative genomics of the Archaea (Euryarchaeota): evolution of conserved protein families, the stable core, and the variable shell. *Genome Res.*, **9**, 608–628.
41. Loris,R., Marianovsky,I., Lah,J., Laeremans,T., Engelberg-Kulka,H., Glaser,G., Muyldermans,S. and Wyns,L. (2003) Crystal structure of the intrinsically flexible addiction antidote MazE. *J. Biol. Chem.*, **278**, 28252–28257.
42. Sullivan,D.M., Bobay,B.G., Kojetin,D.J., Thompson,R.J., Rance,M., Strauch,M.A. and Cavanagh,J. (2008) Insights into the nature of DNA binding of AbrB-like transcription factors. *Structure*, **16**, 1702–1713.
43. Bobay,B.G., Andreeva,A., Mueller,G.A., Cavanagh,J. and Murzin,A.G. (2005) Revised structure of the AbrB N-terminal domain unifies a diverse superfamily of putative DNA-binding proteins. *FEBS Lett.*, **579**, 5669–5674.
44. Lavery,R., Moakher,M., Maddocks,J.H., Petkeviciute,D. and Zakrzewska,K. (2009) Conformational analysis of nucleic acids revisited: Curves+. *Nucleic Acids Res.*, **37**, 5917–5929.
45. Dao-Thi,M.-H., Charlier,D., Loris,R., Maes,D., Messens,J., Wyns,L. and Backmann,J. (2002) Intricate interactions within the ccd plasmid addiction system. *J. Biol. Chem.*, **277**, 3733–3742.
46. Afif,H., Allali,N., Couturier,M. and Van Melderen,L. (2001) The ratio between CcdA and CcdB modulates the transcriptional repression of the ccd poison-antidote system. *Mol. Microbiol.*, **41**, 73–82.
47. Otwinowski,Z., Schevitz,R.W., Zhang,R.G., Lawson,C.L., Joachimiak,A., Marmorstein,R.Q., Luisi,B.F. and Sigler,P.B. (1988) Crystal structure of trp repressor/operator complex at atomic resolution. *Nature*, **335**, 321–329.
48. Rohs,R., Jin,X., West,S.M., Joshi,R., Honig,B. and Mann,R.S. (2010) Origins of specificity in protein-DNA recognition. *Annu. Rev. Biochem.*, **79**, 233–269.
49. Hizver,J., Rozenberg,H., Frolow,F., Rabinovich,D. and Shakked,Z. (2001) DNA bending by an adenine—thymine tract and its role in gene regulation. *Proc. Natl Acad. Sci. USA*, **98**, 8490–8495.
50. Haran,T.E. and Mohanty,U. (2009) The unique structure of A-tracts and intrinsic DNA bending. *Q. Rev. Biophys.*, **42**, 41–81.
51. Olson,W.K., Gorin,A.A., Lu,X.J., Hock,L.M. and Zhurkin,V.B. (1998) DNA sequence-dependent deformability deduced from protein-DNA crystal complexes. *Proc. Natl Acad. Sci. USA*, **95**, 11163–11168.
52. Rohs,R., West,S.M., Sosinsky,A., Liu,P., Mann,R.S. and Honig,B. (2009) The role of DNA shape in protein-DNA recognition. *Nature*, **461**, 1248–1253.
53. Joshi,R., Passner,J.M., Rohs,R., Jain,R., Sosinsky,A., Crickmore,M.A., Jacob,V., Aggarwal,A.K., Honig,B. and Mann,R.S. (2007) Functional specificity of a Hox protein mediated by the recognition of minor groove structure. *Cell*, **131**, 530–543.
54. Stella,S., Cascio,D. and Johnson,R.C. (2010) The shape of the DNA minor groove directs binding by the DNA-bending protein Fis. *Genes Dev.*, **24**, 814–826.
55. Johnson,E.P., Strom,A.R. and Helinski,D.R. (1996) Plasmid RK2 toxin protein ParE: purification and interaction with the ParD antitoxin protein. *J. Bacteriol.*, **178**, 1420–1429.

56. Magnuson,R. and Yarmolinsky,M.B. (1998) Corepression of the P1 addiction operon by Phd and Doc. *J Bacteriol*, **180**, 6342–6351.
57. Garcia-Pino,A., Balasubramanian,S., Wyns,L., Gazit,E., De Greve,H., Magnuson,R.D., Charlier,D., van Nuland,N.A.J. and Loris,R. (2010) Allostery and intrinsic disorder mediate transcription regulation by conditional cooperativity. *Cell*, **142**, 101–111.
58. Edgar,R.C. (2004) MUSCLE: multiple sequence alignment with high accuracy and high throughput. *Nucleic Acids Res.*, **32**, 1792–1797.
59. Luscombe,N.M., Laskowski,R.A. and Thornton,J.M. (1997) NUCPLOT: a program to generate schematic diagrams of protein-nucleic acid interactions. *Nucleic Acids Res.*, **25**, 4940–4945.